Ground effect for ducted wind turbines
A computational study

Sheshadri, Shraddha M.; Dighe, Vinit V.

DOI
10.1088/1742-6596/2265/4/042079

Publication date
2022

Document Version
Final published version

Published in
Journal of Physics: Conference Series

Ground effect for ducted wind turbines: A computational study

Ground effect for ducted wind turbines: A computational study

Shraddha M. Sheshadri[1], Vinit V. Dighe[2]

[1]Renewable Energy Research Group, Department of Aeronautical and Automobile Engineering, Manipal Institute of Technology, India.
[2]Delft Center for Systems and Control, Delft University of Technology, Mekelweg 2, 2628CD Delft, The Netherlands.

E-mail: shraddha.ms@gmail.com

Abstract. Ducted wind turbines (DWTs) can take the advantage of ground effect (GE) when installed close to urban areas. To this aim, a parametric study to investigate the aerodynamic performance of DWTs in relation to three different ground distances are investigated. The flow around a commercial DWT model using a simplified duct actuator disc (AD) model based on Reynolds Averaged Navier-Stokes (RANS) equations is performed. The results indicate that DWTs placed close to the ground will lead to increased mass flow rate the turbine plane, and thereby improving the aerodynamic performance. However, the additional ground force leads to an asymmetric flow-field at the turbine plane, which will ultimately induce unsteady forces on the DWT system. The present analysis will serve as a strong recommendation to address siting issues for DWT manufacturers.

1. Introduction

The recent Intergovernmental Panel on Climate Change (IPCC) report [1], which alarms 'code red for humanity' due to greenhouse gas emissions, highlights the importance of renewable energy for global energy demand. Wind energy will play a key role in the energy transition [2]. Onshore and offshore wind energy has been projected to generate more than one-third (∼35%) of the global electricity needs by the year 2050 [3]. Currently, offshore wind energy contribute a large percentage in the total wind energy production. Integration of wind turbines onshore include challenges, but not limited to: lower wind speed, non-uniform inflow and larger turbulent fluctuations compared to the offshore sites. This results in the reduced onshore installed wind power capacity.

In order to increase the onshore installed wind power capacity, built-environment wind turbines could offer a promising solution [4] for locally produced wind energy similar to a solar photo-voltaic system. One solution could be the use of Vertical Axis Wind turbines (VAWTs) on rooftops, which have the ability to operate in multi-directional flow conditions [5], but have the disadvantage of low efficiency. Small Horizontal Axis Wind Turbines (HAWTs) have also been proposed [6], but suffer from micro-siting and scalability issues [7]. A possible technological solution to extract wind energy in urban areas is represented by Ducted Wind Turbines (DWTs) [8]. A DWT design comprises of a bare wind turbine surrounded by a duct. The role of the duct is to increase the mass flow rate through the turbine relative to a bare turbine operating in the open atmosphere [9]. There are more than one explanation why this occurs [8]. As stated

by de Vries [10], if the sectional lift force of the duct is directed towards the turbine plane, then the associated circulation (see Figure 1) of the duct induces an increased mass flow through the turbine, thereby increasing the generated power.

In reviewing research on DWTs to date [8], we may conclude that ducts can improve the power production of wind turbines in an unbounded flow. Since DWTs are installed close to urban areas, the installation could take advantage of an aerodynamic phenomenon: Ground effect (GE). This phenomenon was studied mainly in the context of amphibian aircraft wings [11]. A close proximity to the water surface leads to increased pressure on the lower surface of the aircraft wings resulting in higher lift coefficient than what is attained in free air stream [12]. The duct designs used in the context of DWTs, in topological space, share a peculiar feature with the aircraft wings: the cross-section of the duct and the aircraft wing represents an airfoil. Theoretically for DWTs, as the lift force on the duct increases due to the underlying pressure, its power output could be further enhanced.

This paper intends to present a detailed parametric study to investigate the GE in relation to the principal design driver - aerodynamic performance. The rest of the paper is organised as follows. Section 2 describes the numerical methodology adopted for the aerodynamic calculations. Section 3 and 4 details the geometric parameters of the DWT models chosen and the numerical setup. Insights on the aerodynamic performance coefficients of the DWT models, in multiple ground settings, are discussed in section 5.

2. Aerodynamics of Ducted Wind Turbines

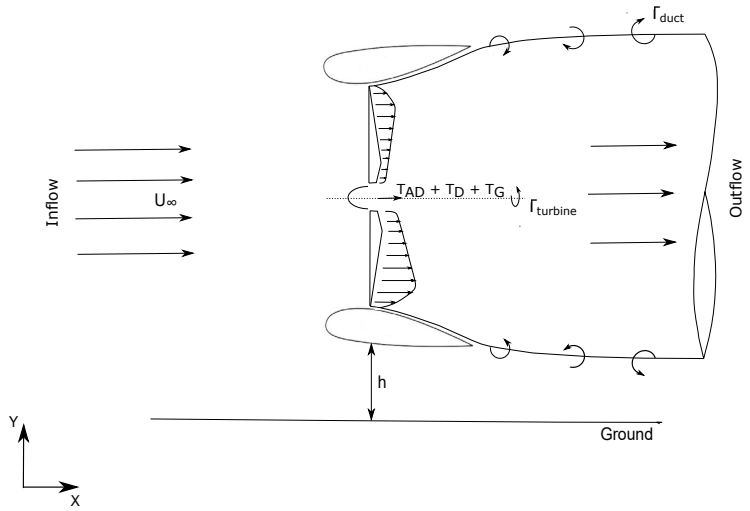

Figure 1: Schematic of flow around a ducted wind turbine in ground effect

Based on the classical actuator disc (AD) theory [13; 14] the flow past a bare wind turbine is represented substituting the rotor with an AD of infinitesimal width. Assuming uniform incompressible flow in steady-state conditions, it is possible to represent the uniform thrust force T_{AD} using a non-dimensional thrust force coefficient:

$$C_{T_{AD}} = \frac{T_{AD}}{\frac{1}{2}\rho U_\infty^2 S_{AD}}, \tag{1}$$

where ρ is the fluid density, U_∞ is the free-stream velocity and S_{AD} is the AD surface area.

A similar approach can be taken to represent the flow past a DWT placed at a close proximity to the ground as shown in Figure 1. In the presence of a DWT close to the ground, additional

thrust forces exerted by the DWT and the ground on the flow, or vice-versa, appears. Then, the total thrust force T is the vectorial sum of the AD thrust force T_{AD}, axial thrust force exerted by the duct T_D and that of the Ground Effect T_G, written as:

$$T = T_{AD} + T_D + T_G \quad and \quad C_T = C_{T_{AD}} + C_{T_D} + C_{T_G}, \tag{2}$$

The presence of duct and GE results in an overall mass flow rate $\dot{m} = \rho S_{AD} U_{AD}$, when calculated across the AD plane. It is worth mentioning that some studies adopt a different definition for mass flow rate calculation in which the reference area is taken at the duct exit section. We will limit our discussion to AD surface area S_{AD}. Although the assumption of constant loading $C_{T\,AD}$ is employed, the free stream velocity computed at the AD plane cannot be regarded as radially uniform; especially for a duct-AD model with GE where the velocity profile becomes asymmetric. In order to account for the non-uniform flow in the radial direction, the mean AD velocity U_{AD} is defined by integrating the differential terms for the local axial velocity U_x across the AD surface:

$$U_{AD} = \frac{1}{S_{AD}} \int_{S_{AD}} U_x dS. \tag{3}$$

Using equation 3, the power coefficient of the duct-AD model placed closed to the ground surface will be written as:

$$C_P = \frac{P}{\frac{1}{2}\rho U_\infty^3 A_{AD}} = \frac{U_{x_{AD}}}{U_\infty} C_{T_{AD}}. \tag{4}$$

3. Methodology

The commercial DonQi® DWT model is selected as reference model for the numerical study; the geometry is made available in [8]. Large Eddy Simulation (LES) method, used in the context of DWT modelling [8], are more likely to be more accurate in approximating the flow around a DWT model. However, the computational cost of LES method render them inappropriate for this parametric study, where extended range of simulations are performed. In contrast, numerical parametric study for DWTs employing vortex panel methods [8; 15] remain computationally advantageous, but inherently insufficient to capture the viscous mutual interactions between the duct and the turbine. Large pressure and velocity gradients are expected for DWTs in GE. To this aim, Reynolds-averaged Navier Stokes (RANS) formulation is chosen, which provides reasonable approximation in capturing the complex viscous flow features, in the context of DWTs, while remaining computationally affordable [8; 15]. A commercial CFD solver ANSYS Fluent is used for computing viscous solutions of steady incompressible flow around DWT using a simplified duct-AD model. Turbulence is modelled using the second-order closure model: $k-\omega$ SST (shear stress transport); the model outperforms the other first and second-order closure models for modelling flow across the duct-AD model [8].

For validating the computational approach, results obtained using two-dimensional (2D) and three-dimensional (3D) simulations for a reference case are compared. The 3D grid is created by extruding the 2D grid in azimuthal direction ϕ using the surface grid extrusion technique [16]. Figure 2 shows the comparison of the free-stream velocity U_x measured behind the AD at $x/c = 0.37$ in the radial direction y. The 2D asymmetric approach gives results of reasonable accuracy when compared to the 3D simulations for a duct-AD model. The computing cost issued by going from 2D to 3D does not justify the scope of the current study, where the effects of distributed AD loading, wake rotation and divergence are totally ignored. Having said that, the 2D approach combined with numerical duct-AD model shown in Figure 3 has been adopted for the results presented, hereinafter.

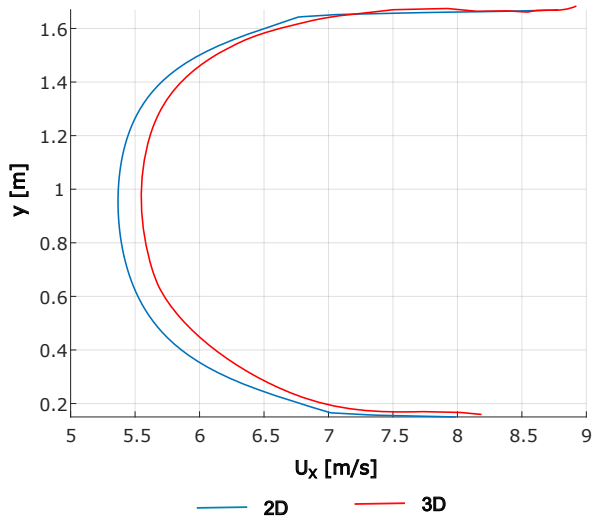

Figure 2: Comparison of the free-stream velocity U_x measured behind the AD at $x/c = 0.37$ in the radial direction y using 2D and 3D duct-AD model for a ground distance h/c = 4 and $C_{T_{AD}}$ = 0.8.

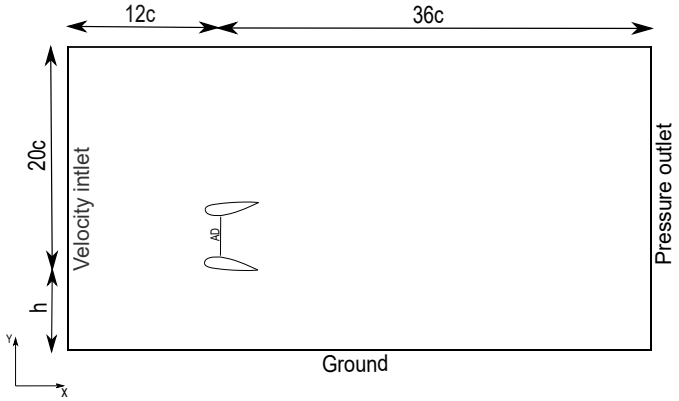

Figure 3: Computational domain with the boundary conditions employed (representative, not to scale)

The domain distances are normalised with the duct chord length c. The distances from the AD location to domain inlet and outlet are $12c$ and $36c$ respectively. h is the variable distance from the ground; the chosen values will be discussed in section 5. Boundary conditions are: uniform velocity inlet at the inlet, zero gauge static pressure outlet at the outlet and no-slip walls for the duct surfaces and the ground. The influence of the pressure drop created by the AD is included into the domain as an additional body force acting opposite to the direction of flow. This is achieved using a reverse fan boundary condition in ANSYS Fluent® taking the uniform thrust loading, the thrust force is given by:

$$T_{AD} = 0.5 C_{T_{AD}} \rho U_{\infty}^2, \tag{5}$$

where $C_{T_{AD}}$ is calculated from a semi-empirical relation of pressure drop curve and the free stream velocity is selected from wind tunnel experiment reported [17]. The fluid is air with fluid density $\rho = 1.225 \frac{kg}{m^3}$ and dynamic viscosity $\mu = 1.7894 \times 10^{-5}$ $Pa{\cdot}s$. Values of free-stream

velocity $U_\infty = 6ms^{-1}$ and turbulence intensity $I = 13.5\%$ are chosen based on the reference values for small urban wind turbine study [18]. The value of AD loading is taken from 0.4 to 1.1 with increments of 0.1. The numerical study is performed at a fixed Re of 4.5×10^5.

The continuity and the momentum equation are solved using the pressure-based solver. The RANS solutions are obtained using the coupled algorithm; it offers robustness and faster convergence for steady solutions in comparison to the segregated solution schemes. A least-squares cell-based method is used to evaluate the pressure gradient, with continuity and momentum equations solved using a second order upwind differential scheme. The convergence criteria is set to 10^{-6} for all the residuals. A typical RANS converged solution with approximately 0.05 million mesh elements is obtained in roughly 0.5 hours on a quad-core work-station desktop computer.

4. Grid Independence Study

The computational grid consists of quadrilateral cells with maximum $y^+ < 5$ on the duct walls [8]. A C-grid structured zonal approach is chosen, which proved advantageous in the case of a curved duct boundaries; see Figure 4. The C-shaped loop terminates in the wake region. Bi-geometric bunching law is applied along the edges of the curved boundary, which generates a finer mesh resolution along the duct's leading and trailing edge regions.

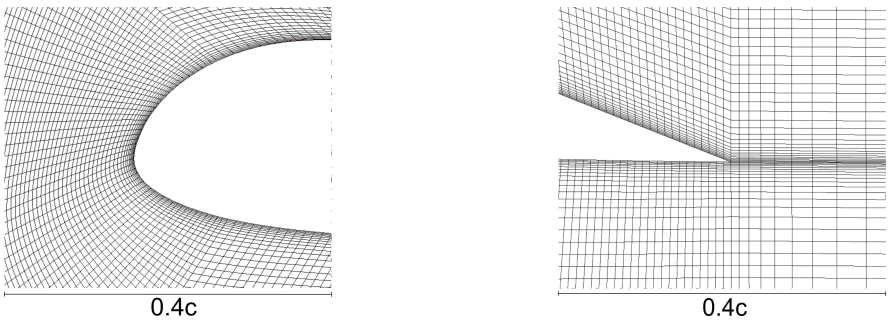

Figure 4: Computational grid along the leading and trailing edge of the duct

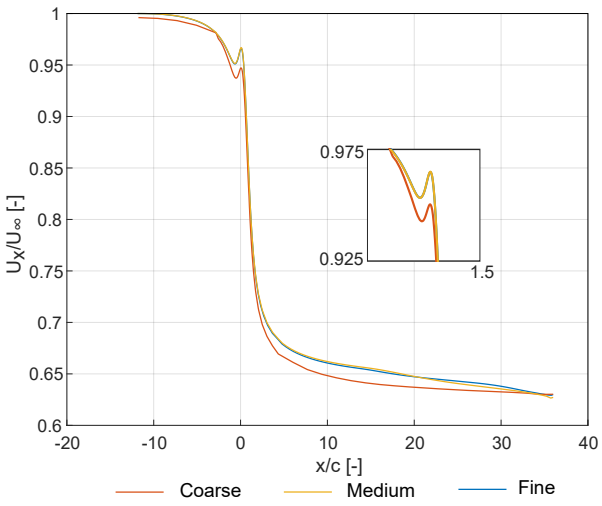

Figure 5: Grid Independence Study showing normalised centre line axial velocity measured across the computational domain

To ensure grid independent solutions, the effect of mesh refinement on the $\frac{U_x}{U_\infty}$ obtained for the flow both upstream and downstream of the AD (center-line) is studied; this is shown in Figure 5. The baseline DonQi® duct-AD model with $C_{TAD} = 0.7$ is chosen for the analysis. Moreover, the ground distance $\frac{h}{c} = 3$ is kept constant throughout the analysis. Three grid sizes (coarse = 30000 elements, medium = 50000 elements and fine = 70000 elements), where the refinement factor in each direction is approximately 1.25, are chosen. The computed $\frac{U_x}{U_\infty}$ trend-lines, in Figure 5, show a local maxima at $h/c = 0$. $\frac{U_x}{U_\infty}$ decreases gradually beyond the local maxima and represents the wake region. $h/c = 0$ corresponds to the AD location in the nozzle plane of the duct. Convergence in the grid independence study is reached in this area for the medium grid and is used for the rest of the paper. The negligible difference can be attributed to the iterative convergence error or the computer round-off error.

5. Results and discussions

This section provides an analysis to study GE in relation to the performance (C_P) of the DonQi® DWT model, as a function of variable AD loading ($C_{T_{AD}}$). To this aim, three ground distances (h/c) = 2, 4 and 6 have been studied. This selection is based on [19] studying optimum tower length while referring to various roof mounted small wind turbines [20]. Some insights on the changes occurring to the performance coefficient are obtained through the flow analysis in this section.

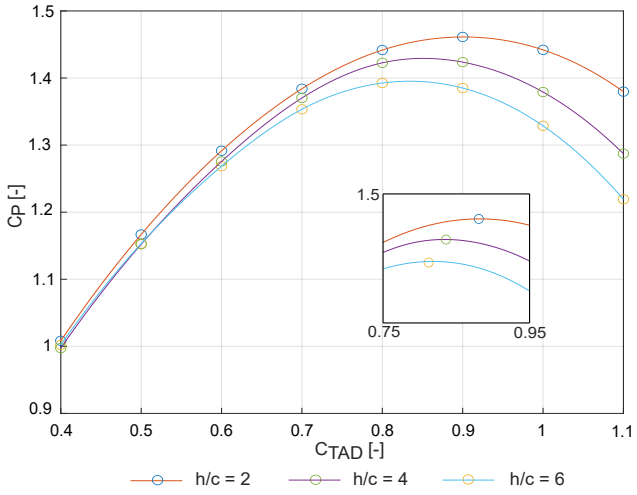

Figure 6: Effect of AD thrust coefficient ($C_{T_{AD}}$) on the Power coefficient (C_P) measured for ground distances $h/c = 2$, 4 and 6.

Figure 6 illustrates the correlation between C_P and $C_{T_{AD}}$ for three different h/c values. In general, C_P value increases with the increasing $C_{T_{AD}}$. Subsequently, a local C_P maxima for different values of h/c appears. The value of C_P decreases for $C_{T_{AD}}$ beyond the local maxima.

Overall, the C_P obtained challenges the well-known Betz-Lanchester-Joukowsky limit of 0.593 [21] for maximum power coefficient obtainable for a bare wind turbine. This should not appear like a surprising result, since, the mass flow of air swallowed by a DWT is greater due to the additional thrust force offered by the duct. Moreover, as shown in equation 2, the GE increases the overall downwind thrust force on the DWT, and thereby resulting in higher C_P for decreasing value of h/c (see Figure 6).

Interestingly, present results show that the maximum C_P for $h/c = 2$ is obtained for a $C_{T_{AD}} \approx 0.89$, viz. Betz limit. This contradicts the conclusion stated in [22] that the optimal $C_{T_{AD}}$ for DWTs will always be lower than 0.89. This is because, the performance of the DWT studied in [22; 23] account for the mutual and nonlinear interactions between the duct and the AD (turbine) thrust forces in an unbounded flow. In real-world conditions, for e.g. building/roof mounted DWTs, the additional GE thrust force needs to be accounted for calculating the DWTs performance.

In order to highlight the GE on C_P for different h/c values shown above, a flow field analysis using RANS solutions is carried out. Velocity contours colored with normalised free stream velocity $\frac{U_x}{U_\infty}$ are shown in Figure 7. Contours are plotted on a plane close to the surface of the duct-AD model and ground, thus allowing a better interpretation of the flow field associated with GE interactions. For the flow analysis, $C_{T_{AD}} = 0.7$ is considered. For $h/c = 2$, high pressure area, characterised by reduced velocity, remain persistent outside of the duct surface on the side that is close to the ground. The high pressure area, when seen outside of the duct surface, contribute positively to the velocity at the AD (see equation 3) and ultimately the C_P (see equation 4). The velocity contours show that, with the increasing value of h/c, the high pressure area present on the outside of the duct (ground side) reduces characterised by higher velocity on the outside of the duct, and thereby resulting in reduced integrated duct thrust force. As a consequence of this, reduced flow is drawn at the AD for $h/c = 4$ and 6, subsequently.

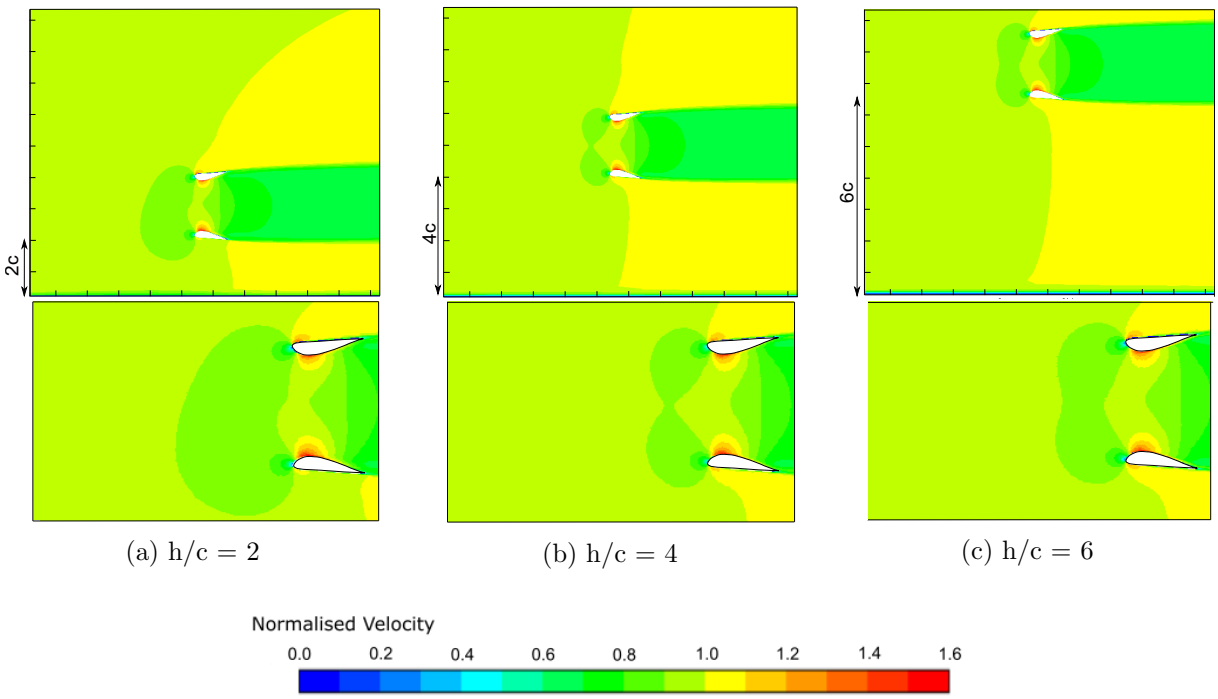

(a) h/c = 2 (b) h/c = 4 (c) h/c = 6

Figure 7: Velocity contours with magnified views emphasising the flow field at the AD coloured with streamwise normalised velocity. The results are depicted for DonQi® duct-AD model bearing a constant $C_{T_{AD}} = 0.7$

Based on the data published by NREL [24] for utility scale urban wind turbines, the tower and foundation costs account for 38% of the overall system capital costs [25]. The key cost drivers identified for tower and foundation costs are, but not limited to: tower and foundation design, materials, available on-site space and local/governmental legislation for tower height requirements. Using GE, based on the analysis shown above, it is possible to significantly

increase the performance of the DWTs by placing it close to the ground with a reduced tower height. However it should be noted that placing DWTs very close to the ground would involve some risk. The GE will cause asymmetric flow-field at the AD (turbine) plane as seen in Figure 2, $h/c = 4$, which will induce unsteady forces on the DWT system, thus increasing the possibility of mechanical failures.

6. Conclusions

In this article, ground effect (GE) for DWTs is studied based on a parametric study. To this aim, two-dimensional numerical calculations using RANS simulations are performed. Based on the existing studies, three ground distances (h/c = 2, 4 and 6) are chosen. These distances are studied under varying AD loadings, viz. $C_{T_{AD}}$ = 0.4-1.1. The results show that the power coefficient C_P for the DWT increases with increasing $C_{T_{AD}}$ upto a point where a local C_P maxima for different ground distances appear. The value of C_P decreases for $C_{T_{AD}}$ beyond the local maxima. The DWT placed at $h/c = 2$ returns the highest C_P with a 5.8% increment at $C_{T_{AD}} = 0.9$ when compared with $h/c = 6$. Flow contours reveal that the additional thrust force exerted by the ground induces an increased mass flow at the the AD surface. However, the observed flow field across the AD surface for $h/c = 2$ appear to be asymmetric, which might induce unsteady loadings on the DWT system.

This research further opens horizons for DWT developers and manufacturers to address DWT siting issues. In the future, the results of this study can be further validated using high fidelity LES simulations or experiments.

References

[1] Paola Arias, Nicolas Bellouin, Erika Coppola, Richard Jones, Gerhard Krinner, Jochem Marotzke, Vaishali Naik, Matthew Palmer, G-K Plattner, Joeri Rogelj, et al. Climate change 2021: The physical science basis. contribution of working group14 i to the sixth assessment report of the intergovernmental panel on climate change; technical summary. 2021.

[2] Ryan Wiser, Joseph Rand, Joachim Seel, Philipp Beiter, Erin Baker, Eric Lantz, and Patrick Gilman. Expert elicitation survey predicts 37% to 49% declines in wind energy costs by 2050. *Nature Energy*, 6(5):555–565, 2021.

[3] IREA IRENA. Future of wind: Deployment, investment, technology, grid integration and socio-economic aspects. 2019.

[4] Petar Škvorc and Hrvoje Kozmar. Wind energy harnessing on tall buildings in urban environments. *Renewable and Sustainable Energy Reviews*, 152:111662, 2021.

[5] Francisco Toja-Silva, Antonio Colmenar-Santos, and Manuel Castro-Gil. Urban wind energy exploitation systems: Behaviour under multidirectional flow conditions—opportunities and challenges. *Renewable and Sustainable Energy Reviews*, 24:364–378, 2013.

[6] Aikaterini Konstantina Chrysochou. *Urban wind turbines-a literature review on current research*. PhD thesis, Wien, 2021.

[7] KC Anup, Jonathan Whale, and Tania Urmee. Urban wind conditions and small wind turbines in the built environment: A review. *Renewable energy*, 131:268–283, 2019.

[8] Vinit Dighe. *Ducted wind turbines revisited: A computational study*. PhD thesis, Delft University of Technology, Delft, The Netherlands, 2009.

[9] Gerard J W van Bussel. The science of making more torque from wind: Diffuser experiments and theory revisited. 2007.

[10] O de Vries. Fluid dynamic aspects of wind energy conversion. Technical report, Advisory Group for Aerospace Research and Development NEUILLY-SUR-SEINE (France), 1979.

[11] Kirill V Rozhdestvensky. Wing-in-ground effect vehicles. *Progress in aerospace sciences*, 42(3):211–283, 2006.

[12] KV Rozhdestvensky. Ekranoplans-the gems of fast water transport. *International Maritime Technology*, 109(pt 1):47–74, 1997.

[13] William John Macquorn Rankine. On the mechanical principles of the action of propellers. *Transactions of the Institution of Naval Architects*, 6, 1865.

[14] Robert Edmund Froude. On the part played in propulsion by differences of fluid pressure. *Trans. Inst. Naval Architects*, 30:390, 1889.

[15] R Bontempo and M Manna. Effects of the duct thrust on the performance of ducted wind turbines. *Energy*, 99:274–287, 2016.

[16] ANSYS Fluent. 14.0 user's manual. *ANSYS Inc., Canonsburg, PA*, 2011.

[17] Juan Tang, Francesco Avallone, and GJW van Bussel. Experimental study of flow field of an aerofoil shaped diffuser with a porous screen simulating the rotor. *International Journal of Computational Methods and Experimental Measurements*, 4(4):502–512, 2016.

[18] QA Li, Junsuke Murata, Masayuki Endo, Takao Maeda, and Yasunari Kamada. Experimental and numerical investigation of the effect of turbulent inflow on a horizontal axis wind turbine (part i: Power performance). *Energy*, 113:713–722, 2016.

[19] Soufiane Karmouche. Tower design and analysis for a small wind turbine. 2016.

[20] Shruti Mohandas Menon and Navid Goudarzi. Structural analysis of a novel ducted wind turbine. In *ASME Power Conference*, volume 57618, page V002T12A003. American Society of Mechanical Engineers, 2017.

[21] Valery L Okulov and Gijs AM Van Kuik. The betz–joukowsky limit: on the contribution to rotor aerodynamics by the british, german and russian scientific schools. *Wind Energy*, 15(2):335–344, 2012.

[22] Vinit V Dighe, Gael de Oliveira, Francesco Avallone, and Gerard JW van Bussel. Characterization of aerodynamic performance of ducted wind turbines: A numerical study. *Wind Energy*, 22(12):1655–1666, 2019.

[23] R Bontempo, R Carandente, and M Manna. A design of experiment approach as applied to the analysis of diffuser-augmented wind turbines. *Energy Conversion and Management*, 235:113924, 2021.

[24] Tyler Stehly, Philipp Beiter, and Patrick Duffy. 2019 cost of wind energy review. Technical report, National Renewable Energy Lab.(NREL), Golden, CO (United States), 2020.

[25] DN Valyou and KD Visser. Design considerations for a small ducted wind turbine. In *Journal of Physics: Conference Series*, volume 1452, page 012019. IOP Publishing, 2020.